Dynamic properties of a polaron coupled to dispersive optical phonons

J. Bonča and S. A. Trugman

Phys. Rev. B **103**, 054304 — Published 12 February 2021

DOI: 10.1103/PhysRevB.103.054304

Dynamic Properties of a Polaron Coupled to Dispersive Optical Phonons

J. Bonča[1,2] and S. A. Trugman[3]

[1]*J. Stefan Institute, 1000 Ljubljana, Slovenia*
[2]*Faculty of Mathematics and Physics, University of Ljubljana, 1000 Ljubljana, Slovenia*
[3]*Theoretical Division, Los Alamos National Laboratory, Los Alamos, New Mexico 87545, USA*

(Dated: February 2, 2021)

We study static and dynamic properties of an electron coupled to dispersive quantum optical phonons in the framework of the Holstein model defined on a one–dimensional lattice. Calculations are performed using the Lanczos algorithm based on a highly efficient construction of the variational Hilbert space. Even small phonon dispersion has a profound effect on the low energy optical response. While the upward phonon dispersion broadens the optical spectra due to single phonon excitations, the downward dispersion has the opposite effect. With increasing dispersion a multi–phonon excitation (MPE) state becomes the lowest excited state of the system at zero momentum and determines the low–frequency response of the optical conductivity where the threshold for optical absorption moves below the single–phonon frequency. Multi–phonon states form a well defined band–like feature just above the polaron band as clearly seen in the electron spectral function. Low–energy MPEs should be observable in systems with strong optical phonon dispersion in optical as well as angle resolved photoemission experiments.

PACS numbers:

I. INTRODUCTION

Interaction between electron and lattice degrees of freedom represents one of the fundamental paradigms in modern solid state physics. In this context the Holstein model (HM)[1] is commonly used to study the interaction between an electron and dispersionless optical phonons. Despite its simplicity, a body of past as well as recent works have been devoted to this model ranging from variational approaches[2–14] and diagrammatic techniques,[15–17] among which the momentum averaged approximation has been particularly successful for the description of static as well as dynamic properties of the model.[18–22] Early exact diagonalization approaches on finite lattices[23–29] have been followed by various Monte Carlo methods.[30–33] In this class of approaches a combined diagrammatic and world line Monte Carlo method[34] has been applied to determine the mobility of an electron subject to local lattice vibrations. Density–matrix renormalization–group techniques[35,36] represent yet another class of advanced techniques most successful in tackling the Holstein model in one spatial dimension. Recently, this approach has been extended to obtain spectral properties of the HM at finite temperatures.[37] In the limit of infinite dimension dynamical mean field approaches[38,39] dominate the research in this field.

One of the most commonly used simplifications in treating electron–phonon interaction based on the HM is to assume that optical phonons are dispersionless, which results in a singular phonon density of states. While a straightforward generalization of the model is the introduction of dispersion among localized (Einstein) phonons, there exist surprisingly few attempts in the literature in this direction. Coupling of the electron to acoustic phonons has been treated using perturbative approaches.[40,41] More related to our present study is the research in Ref.[42] where authors have investigated the influence of the dispersion among optical phonons on the polaron effective mass.

Phonon dispersion also has a profound effect on the propagation of an electron in a one dimensional disordered system. Coupling of the particle to dispersive optical phonons leads to delocalization of the particle by virtue of a subdiffusive spread from the initially localized state while in the case of coupling to dispersionless phonons the particle remains localized.[43] Recently, an important influence of phonon dispersion on the formation of charge density wave order has been demonstrated in a system with finite electron density using the Quantum Monte Carlo technique.[44]

The work described here investigates dynamic properties of an electron coupled to dispersive optical phonons in the context of the HM in one spatial dimension. It is rather surprising that despite a multitude of research devoted to the HM with dispersionless optical phonons, there is a lack of investigations describing the influence of phonon dispersion on dynamic quantities such as the optical conductivity and the electron spectral function. The absence of research could be either due to difficulties introduced by extra terms in the Hamiltonian or due to a common belief that the phonon dispersion does not lead to any unexpected new phenomena.

Our research was motivated in part by recent measurements of the Holstein polaron spectral function in a surface doped layered semiconductor MoS_2.[45] In most materials the bandwidth of optically dispersive phonons is much smaller than the position of the middle of the optical band. A large dispersion of optical phonons can be expected in systems where intracellular interactions are comparable to those between cells, and where the atomic masses do not differ greatly. One such example are GaLaAs superlattice systems where the ratio between maximum and minimum optical frequency is roughly $\omega(0)/\omega(q_{\rm min}) \sim 1.2$.[46] Moreover, in the hexagonal nitride AlN semiconductor, with the C^4_{6v} space group symmetry the lowest optical mode E_2 shows strong upward dispersion along Γ–K direction with the ratio $\omega(K)/\omega(\Gamma) \sim 2.2$ and downward dispersion along the Γ–A direction where $\omega(\Gamma)/\omega(A) \sim 1.7$.[47]

In this work we show that introduction of dispersion among

optical phonons can have a profound effect on the excited states of the model. Even small phonon dispersion has a significant effect on the low energy optical response and the quasiparticle band dispersion observed in the electron spectral function. Upward phonon dispersion broadens the optical spectra due to single phonon excitations. In contrast, the downward dispersion narrows contributions of single and multiple phonon excitations rendering them more easily detectable in the optical response.

While in the dispersionless HM the lowest excited state consists of a polaron and an extra phonon excitation with zero momentum, at large phonon dispersion MPEs from the edge of the Brillouin zone form the lowest excited states that are optically active. They shift the threshold of the optical absorption spectra towards frequencies below the single phonon excitation frequency. A large phonon dispersion renders multi–phonon states observable in the electron spectral function where they obtain a significant spectral weight just above the polaron band.

The paper is organized as follows. In Section II we present the model and give a brief description of the method. In Section III we first introduce dynamic quantities such as the optical conductivity and the electron spectral function. In Subsection III A we present results of various static quantities where a special emphasis is on the description of dispersion relations of a few lowest energy bands. In Subsection III B we analyze the influence of phonon dispersion on the optical conductivity and the electron spectral function. In Section IV we give concluding remarks.

II. MODEL AND METHOD

We analyze a single electron coupled to dispersive optical phonons on an infinite one–dimensional system

$$\begin{aligned} H &= -t_{\rm el}\sum_j (c_j^\dagger c_{j+1} + {\rm H.c.}) + g\sum_j \hat{n}_j(a_j^\dagger + a_j) + \\ &+ t_{\rm ph}\sum_j (a_j^\dagger a_{j+1} + {\rm H.c.}) + \omega_0 \sum_j a_j^\dagger a_j, \end{aligned} \quad (1)$$

where $c_j^\dagger$ and $a_j^\dagger$ are electron and phonon creation operators at site j, respectively, $\hat{n}_j = c_j^\dagger c_j$ represents the electron density operator and $t_{\rm el}$ the nearest-neighbor hopping amplitude. ω_0 denotes the position of the center of the dispersive optical phonon band $\omega(q) = \omega_0 + 2t_{\rm ph}\cos(q)$. We also introduce the dimensionless effective electron-phonon coupling strength $\lambda = \epsilon_{\rm p}/2t_{\rm el} = g^2/2t_{\rm el}\sqrt{\omega_0^2 - 4t_{\rm ph}^2}$ where $\epsilon_{\rm p}$ is the polaron energy in the limit $t_{\rm el} = 0$.[42]

We have used a numerical method described in detail in Refs.[4,5] The method generates the variational Hilbert space starting from the initial single-electron Bloch state $c_k^\dagger|\emptyset\rangle$ where $c_k^\dagger = \frac{1}{\sqrt{L}}\sum_j e^{ikj}c_j^\dagger$, with no phonons on an infinite lattice. The variational Hilbert space is then generated by applying the first two off-diagonal terms of Hamiltonian in Eq. (1), representing the electron kinetic energy and the electron–phonon coupling term, N_h times. In the intermediate coupling regime the method provides computation of the ground state energy in the thermodynamic limit to extremely high accuracy, better than ~ 22 digits. Even though the method is based on an infinite one–dimensional lattice, the constructed variational Hilbert space allows only a finite maximal distance of a phonon quanta from the electron position, $L_{\rm max} = N_{\rm h} - 1$. This limitation is in turn responsible for a discrete phonon dispersion $\omega(q)$. Furthermore, the maximal amount of phonon quanta at the electron position is given by $N_{\rm phmax} = N_{\rm h}$ while on the $M-{\rm th}$ neighboring site to the electron, it is reduced to $N_{\rm phmax} = N_{\rm h} - M$. We have used a standard Lanczos procedure[48] to obtain static as well as dynamic properties of the model.

We have performed numerical calculations in the parameter regime given by $\omega_0/t_{\rm el} \geq 0.5$ and $\lambda \leq 2.0$, where our numerical approach gives most reliable results. In the adiabatic regime, i.e. $\omega_0/t_{\rm el} \to 0$ other semi–classical approaches are possibly more adequate. In addition, we have limited our calculations to one spatial dimension even though calculations at higher dimensions are possible using our approach as have been shown for static properties in Ref.[5].

III. RESULTS

Our main focus is on dynamic properties of the model. We first present common formulas for the real part of the optical conductivity, based on the linear response theory. For the specific model Hamiltonian in Eq. (1) the real part of the optical conductivity can be written in two parts ${\rm Re}\sigma(\omega) = D\delta(\omega) + \sigma^{\rm reg}(\omega)$ where the Drude weight, also known as the charge stiffness D, represents the ballistic response of a system. The regular part $\sigma^{\rm reg}(\omega)$ corresponds to the absorption of an AC field

$$\sigma^{\rm reg}(\omega) = \frac{\pi}{\omega}\sum_n |\langle\psi_0^{(n)}|\hat{j}|\psi_0^{(0)}\rangle|^2\delta(\omega - (E^{(n)}(0) - E^{(0)}(0))) \quad (2)$$

where $\hat{j} = -it_{\rm el}\sum_i c_{i+1}^\dagger c_i - c_i^\dagger c_{i+1}$ is the current operator while $\psi_0^{(n)} = \psi_{k=0}^{(n)}$ are many–body eigenstates and $E^{(n)}(0) = E^{(n)}(k=0)$ corresponding energies computed at zero momentum and n indicates the n-th excited state. The Drude weight can be determined from the following expression

$$D = -\langle\psi_0^{(0)}|H_{\rm kin}|\psi_0^{(0)}\rangle/2 - \sum_{n\neq 0}\frac{|\langle\psi_0^{(0)}|\hat{j}|\psi_0^{(n)}\rangle|^2}{E^{(n)}(0) - E^{(0)}(0)}, \quad (3)$$

where $H_{\rm kin}$ represents the first term in Eq. 1. Alternatively, D can as well be determined from the properties of polaron dispersion relation $D = \frac{1}{2}{\rm d}^2E^{(0)}(k)/{\rm d}k^2|_{k=0}$, which can serve as a test of the method. Note also that $\int_0^\infty {\rm Re}\sigma(\omega){\rm d}\omega = -\frac{\pi}{2}\langle\psi_0^{(0)}|H_{\rm kin}|\psi_0^{(0)}\rangle$ represents the so called optical sum–rule. Note that the optical spectral weight due to the optical phonons themselves is not included. One way to think of this is that we are modeling the case where the tight-binding lattice is in the $x-$direction, the external applied electric field is also

in the $x-$direction, and the optical phonon ion displacement is in the $y-$direction.

We also define the electron addition spectral function

$$A(\omega,k)=\sum_n |\langle\psi_k^{(n)}|c_k^\dagger|\emptyset\rangle|^2\delta(\omega-E^{(n)}(k)), \qquad (4)$$

where $|\emptyset\rangle$ represents the electron and phonon vacuum.

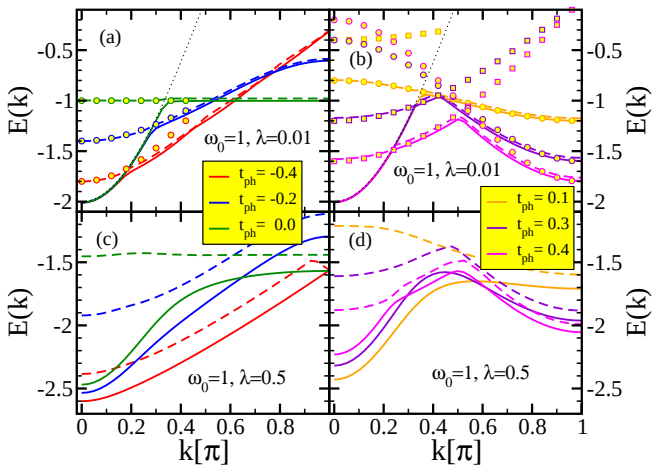

Figure 1: The energy band $E^{(0)}(k)$ (full lines) and the first excited state energy $E^{(1)}(k)$ (dashed lines) computed at $\omega_0=1$, $\lambda=0.01$ in a) and b) and $\lambda=0.5$ in c) and d). Open circles in a) and b) denote $E_{1\rm ph}(k)=-2t_{\rm el}+\omega_0+2t_{\rm ph}\cos(k)$ while open squares in b) $E_{2\rm ph}(k)=-2t_{\rm el}+2\omega_0-4t_{\rm ph}\cos(k/2)$. In this and in all subsequent figures we set $t_{\rm el}=1$ as the unit of energy. Tiny dotted line in a) and b) denotes the free electron energy $E_{\rm free}(k)$. In this and in all subsequent figures we have used $N_{\rm h}=18$.

A. Static properties

We start with the analysis of the low–lying energy spectra. In Fig. 1 we present the expectation value of the lowest energy band $E^{(0)}(k)=\langle\psi_k^{(0)}|H|\psi_k^{(0)}\rangle$ and the first excited energy band $E^{(1)}(k)=\langle\psi_k^{(1)}|H|\psi_k^{(1)}\rangle$ using different values of $t_{\rm ph}$. We have explored the whole range of $|t_{\rm ph}|<\omega_0/2$. We should also keep in mind that $t_{\rm ph}>0$ represents the downward dispersion relation of optical phonons. We first analyze results in the limit $\lambda\to 0$, presented in Figs. 1(a) and (b). In all cases $E^{(0)}(k)$ at small momentum approximately follows the free electron dispersion relation $E^{(0)}(k)\sim E_{\rm free}(k)=-2t_{\rm el}\cos(k)$. For $t_{\rm ph}\le 0$, the lowest energy band at some finite momentum bends over towards $E^{(0)}(k)\sim E_{1\rm ph}(k)=-2t_{\rm el}+\omega_0+2t_{\rm ph}\cos(k)$. This state is composed of a free electron with momentum $k_{\rm el}=0$ and one phonon excitation with momentum k.[49] This holds true up to $t_{\rm ph}=0.1$. Naively, one would expect that the first excited state at zero momentum always consists of an additional single phonon excitation which would yield an excitation gap at $k=0$: $\Delta E=\omega_0+2t_{\rm ph}$. In contrast, at $t_{\rm ph}=0.3$ and 0.4 we observe a significant decrease of the energy of the first excited state which is due to a state that consists of an electron with momentum $k_{\rm el}=0$ and two phonon excitations with identical momenta $q_1=q_2=\pi+k/2$ yielding a total momentum $k=k_{\rm el}+2q_1$ and the excitation energy $E_{2\rm ph}(k)=-2t_{\rm el}+2\omega_0-4t_{\rm ph}\cos(k/2)$. For $t_{\rm ph}=0.3$ and 0.4 $E^{(0)}(k)$ with increasing k bends over from $E_{\rm free}(k)$ towards the two–phonon energy $E_{2\rm ph}(k)$ then to $E_{1\rm ph}(k)$, which gives rise to a somewhat unusual dispersion relation. From the condition $E_{2\rm ph}(k=0)=E_{1\rm ph}(k=0)$ we obtain the threshold value $t_{\rm ph}^{\rm th}(M_{\rm ph}=2)=\omega_0/6$ when the two phonon excitation energy first appears below the one phonon one. Multiple crossings also explain the polaron dispersion relation at $\lambda=0.5$ as shown in Fig. 1(c) and (d).

Note also that higher excited states, not shown in Fig. 1, with $M_{\rm ph}=4,6,\ldots$ number of even phonon excitations with $q_{M_{\rm ph}}=\pi+k/M_{\rm ph}$ lie below a single phonon excitation with $q=k$ around $k\sim 0$ as long as $t_{\rm ph}^{\rm th}(M_{\rm ph})\ge(M_{\rm ph}-1)\omega_0/\left(2(M_{\rm ph}+1)\right)$. In the case when $t_{\rm ph}=0.4\omega_0$ there exist $M_{\rm ph}=2,4,\ldots,8$ MPEs below the single phonon one since $t_{\rm ph}^{\rm th}(M_{\rm ph}=8)=0.39\omega_0$.

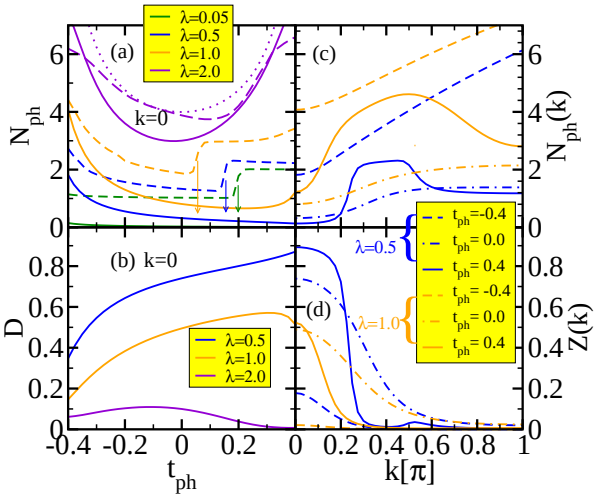

Figure 2: a) the expectation number of phonons $N_{\rm ph}^{(0,1)}$ in the ground (full lines) and excited (dashed lines) state vs. $t_{\rm ph}$ for four different values of λ and zero momentum. The dotted line represents the strong coupling prediction[42] $N_{\rm ph}^{\rm sc}$, given in the text. Arrows indicate threshold values $t_{\rm ph}^{\rm th}(M_{\rm ph}=2)$; b) the Drude weight vs. $t_{\rm ph}$; c) $N_{\rm ph}^{(0)}(k)$ computed for two different values of $\lambda=0.5$ and 1 and three different values of $t_{\rm ph}=\pm 0.4$ and 0; d) $Z(k)$ computed using identical parameters as in c). In all cases the phonon frequency is set to $\omega_0=1$.

The existence of the two–phonon first excited state is further analyzed by computing the expectation number of phonons $N_{\rm ph}^{(n)}(k)=\langle\psi_k^{(n)}|\sum_i a_i^\dagger a_i|\psi_k^{(n)}\rangle$ in the ground and the first excited state, $n=0$ and 1, respectively. At small $\lambda=0.05$ we observe a sudden jump in $N_{\rm ph}^{(1)}(k=0)$ by $\Delta N_{\rm ph}^{(1)}(k=0)\sim 1$ around $t_{\rm ph}\sim 0.18$ that is very close to the analytical estimate $t_{\rm ph}^{\rm th}(M_{\rm ph}=2)=0.17$. The difference is due to a small finite–size effect.[50] With increasing

λ, up to $\lambda \sim 1.0$, the effective $t_{\rm ph}^{\rm th}(M_{\rm ph}=2)$ scales with λ as it shifts significantly towards smaller, physically more relevant values. For $\lambda = 1$ we obtain $t_{\rm ph}^{\rm th}(M_{\rm ph}=2) \sim 0.06$, which yields the ratio $\omega(\pi)/\omega(0) \sim 1.27$. Consequently, in the intermediate electron–phonon coupling regime, MPEs can be observed already at relatively small optical phonon dispersion. The ground state $N_{\rm ph}^{(0)}(k=0)$ decreases as $t_{\rm ph}$ increases around $t_{\rm ph}=0$ and shows no significant change in the vicinity of $t_{\rm ph}^{\rm th}$. In the strong coupling regime, at $\lambda = 2.0$, the two–phonon excitation above the ground state crosses over to a state with nearly identical values of $N_{\rm ph}^{(0)}(k=0) \sim N_{\rm ph}^{(1)}(k=0)$ for $t_{\rm ph} \gtrsim 0.2$. The ground state $N_{\rm ph}^{(0)}(k=0)$ qualitatively follows the strong coupling prediction[42] $N_{\rm ph}^{\rm sc} = 2t_{\rm el}\omega_0\lambda/\sqrt{\omega_0^2-4t_{\rm tp}^2}$.

In Fig. 2(b) we present the Drude weight that as expected decreases with increasing λ while its behavior around $t_{\rm ph}=0$ changes from increasing with $t_{\rm ph}$ in the weak to intermediate coupling regime to decreasing at $\lambda = 2.0$, consistent with results of the effective mass in Ref.[42]. The latter can be understood within the strong coupling limit where $D^{\rm sc} = \exp\left[-2t_{\rm el}\lambda/(\omega_0-2t_{\rm ph})\right]$.

An important difference between the upward $t_{\rm ph} > 0$ and the downward dispersion $t_{\rm ph} < 0$ is also reflected in the lowest energy state momentum dependence of $N_{\rm ph}^{(0)}(k)$, as shown in Fig. 2(c). While $N_{\rm ph}^{(0)}(k)$ monotonically increases with increasing momentum for $t_{\rm ph}=-0.4$, it displays at $t_{\rm ph}=0.4$ a clear non–monotonic momentum dependence. The physics of the latter dependence is most clearly seen from the weak coupling regime at $\lambda = 0.5$, where it starts around zero at $k=0$ then jumps to $N_{\rm ph}^{(0)}(k_1 \sim 0.2\pi) \sim 2$ followed by a drop to $N_{\rm ph}^{(0)}(k_2 \sim 0.6\pi) \sim 1$. The lowest energy wavefunction consists for $k \lesssim k_1$ predominantly of an electron with momentum $k_{\rm el}=k$ then for $k_1 \lesssim k \lesssim k_2$ of an electron with momentum $k_{\rm el}$ near zero and two phonon excitations each with momentum near $q_{1,2} = \pi + k/2$ and finally for $k \gtrsim k_2$ of an electron with $k_{\rm el}$ near zero and a single phonon excitation with $q \sim k$. Such structure of the polaron wavefunction is as well reflected in the quasiparticle weight $Z(k) = |\langle\psi_k^{(0)}|c_k^\dagger|\emptyset\rangle|^2$ as seen in Fig. 2(d) where for $t_{\rm ph}=0.4$ we observe a sudden decrease with k while at $t_{\rm ph}=0.0$ the decrease is much more gradual.

B. Dynamic properties

We shall now investigate whether the existence of multi-phonon excitations affects any measurable quantities, such as the optical conductivity or the spectral function. In Fig. 3 we present $\sigma^{\rm reg}(\omega)$. In the weak coupling regime, *i.e.* at $\lambda = 0.5$ and for $t_{\rm ph} \leq 0.2$ the incoherent absorption spectra starts at $\omega^{\rm 1ph} = \omega_0 + 2t_{\rm ph}$. In particular, at $t_{\rm ph}=-0.2$ we observe a series of peaks that are after the initial increase monotonically decreasing with increasing ω. The response of the system at small ω can be explained by processes where and electron with initial momentum $k_{\rm el}=0$ emits a phonon excitation with momentum q while the electron in this scattering process changes its momentum to $k_{\rm el}=-q$. Contributions due to single–, two– or multiple–phonon excitations can not be distinguished between each other. Discrete peaks appear due to a limited variational Hilbert space that leads to a discrete set of internal momenta q. Additional discussion concerning the numerical precision of the numerical method is provided in Appendix A. At $t_{\rm ph}=0.0$ that represents the standard HM with dispersionless Einstein phonons we already observe two slightly separated groups of peaks whereby the first represents single–phonon emission processes and the second two–phonon ones. Besides a shift towards higher ω with further increasing $t_{\rm ph}$ we observe a substantial narrowing of the single–phonon emission spectra that is followed by another well defined two–phonon emission peak, separated approximately ω_0 from the first one. The narrowing of the spectra at $t_{\rm ph} > 0$ is a consequence of the downward phonon dispersion. In the above described phonon emission process the energy of the emitted phonon at finite q decreases in comparison to $q=0$ which has the effect of narrowing the single–phonon emission spectra in comparison to $t_{\rm ph} \leq 0$. Similar effects are even more pronounced in the intermediate coupling regime, $\lambda = 1.0$.

Even more unexpected is the appearance of the absorption spectra below the one–phonon emission threshold $\omega^{\rm 1ph}$ as in Fig. 3 indicated by vertical full lines with arrows. Dashed lines with arrows indicate the threshold of multi–phonon

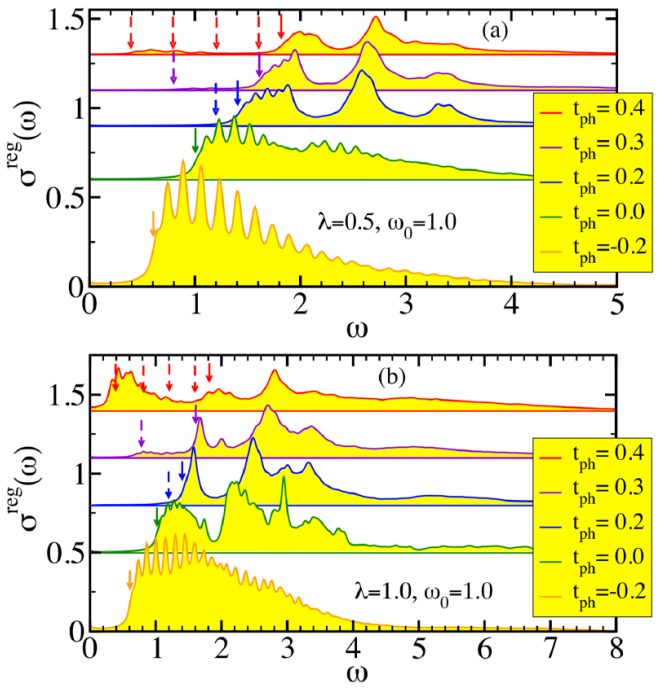

Figure 3: $\sigma^{\rm reg}(\omega)$ computed at $\omega_0=1$ for different $t_{\rm ph}$ as denoted in legends where ω is in units of $t_{\rm el}=1$. Full lines with downward arrows denote positions of the lowest single phonon excitation above the ground state, $\omega^{\rm 1ph} = \omega_0 + 2t_{\rm ph}$, while multiple dashed lines with arrows represent the lowest $M_{\rm ph}=2,4,6$, and 8 phonon excitation $\omega^{\rm Mph} = M_{\rm ph}(\omega_0 - 2t_{\rm ph})$ threshold in all figures where $\omega^{\rm Mph} < \omega^{\rm 1ph}$. We have used artificial broadening $\eta = 0.05$.

emission spectra $\omega^{\mathrm{M_{ph}}} = M_{\mathrm{ph}}(\omega_0 - 2t_{\mathrm{ph}})$ where an electron scatters off an even number of M_{ph} phonons, each with momentum $q = \pi + k/M_{\mathrm{ph}}$ while the electron shifts after scattering from $k_{\mathrm{el}} = 0$ to $k_{\mathrm{el}} = -k$. Optical absorption due to two phonon emission processes obtains a substantial spectral weight at the intermediate coupling regime $\lambda = 1.0$, as seen in Fig. 3 (b).

We continue with the discussion of the electron spectral function. We first present results for a single site, i.e. for $t_{\mathrm{el}} = 0$, where $A(\omega)$ is given by the following expression

$$A(\omega) = e^{-\sum_q \tilde{g}_q^2} \sum_{m_{q_1}, m_{q_2}, \ldots, m_{q_{N_q}}=0}^{\infty} \left[\Pi_q \frac{\tilde{g}^{2m_q}}{m_q!}\right] \delta\left(\omega + \sum_q \omega_q \tilde{g}_q^2 - \sum_q m_q \omega_q\right), \tag{5}$$

where $\tilde{g}_q = \frac{g}{\sqrt{N_q \omega_q}}$, N_q represents the number of discrete q values, the average number of phonon excitations is given by $\bar{N}_{\mathrm{ph}} = \sum_q \tilde{g}_q^2$, the polaron energy spectrum is $\epsilon_p = -\sum_q \omega_q \tilde{g}_q^2 + \sum_q m_q \omega_q$ and the quasiparticle weight can be obtained by setting all $m_{q_i} = 0$, which leads $Z_{\mathrm{qp}} = e^{-\sum_q \tilde{g}_q^2}$. In Appendix B we further elaborate on the derivation of Eq. 5 as well as on some details concerning the numerical summation to obtain $A(\omega)$ as presented in Fig. 4. In the case of zero dispersion $t_{\mathrm{ph}} = 0$, $A(\omega)$ matches well known results for dispersionless phonons.[51,52] The lowest peak is positioned at the ground–state quasiparticle energy $\epsilon_p^0 = -\sum_q \omega_q \tilde{g}_q^2$ while peaks at higher ω represent multi–phonon contributions, spaced by ω_0. All peaks are represented by Lorentzian forms of delta functions with artificial broadening and have zero physical width. At small but finite $t_{\mathrm{ph}} = 0.05$ and 0.1 all peaks except the lowest one obtain a finite width at half maximum W, given by the bandwidth of the phonon spectrum, $W = 4t_{\mathrm{ph}}$. Contributions from one-, two- and multi phonon excitations remain well separated. At even larger t_{ph} contributions from multi phonon excitation start merging into a broad continuum. Notable is also the closing of the gap between the quasi–particle peak and the rest of the spectra.

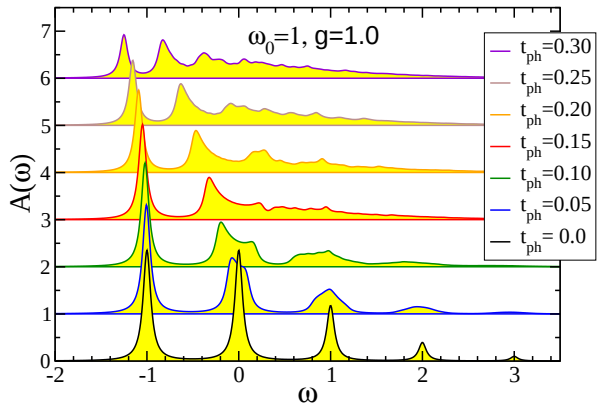

Figure 4: $A(\omega)$ computed from Eq. 5 at $\omega_0 = g = 1$ for different t_{ph} as denoted in legends. Results do not depend on the sign of t_{ph}. We have used $N_q = 10$ and artificial broadening $\eta = 0.05$. For further details see caption of Fig. B1.

The introduction of optical phonon dispersion has a profound effect on the electron spectral functions $A(\omega, k)$ also at $t_{\mathrm{el}} \neq 0$ as presented in the form of density plots in Fig. 5. As guides to the eye we also display with tiny dashed lines the dispersion relations of the lowest energy band marking the position of the polaron band, $E^{(0)}(k)$ as well as the analytical estimate of the single phonon excitation above the lowest energy band: $E_{1\mathrm{ph}}(k) = E^{(0)}(k=0) + \omega_0 + 2t_{\mathrm{ph}} \cos(k)$ using dot–dashed lines shown only in the vicinity of the center of the Brillouin zone.

At small $\lambda = 0.5$, see Figs. 5(a-e), in the case of the upward dispersion, i.e. for $t_{\mathrm{ph}} = -0.2$, the polaron band is monotonically increasing with increasing momentum while the gap between the quasiparticle band and the rest of the incoherent spectrum diminishes in comparison to $t_{\mathrm{ph}} \geq 0.2$. There is a well defined part of the incoherent spectrum above the polaron band around $k = 0$ at the position that corresponds to the single phonon excitation $E_{1\mathrm{ph}}(k)$. For $t_{\mathrm{ph}} \geq 0.2$ the spectral weight of the incoherent part around $E_{1\mathrm{ph}}(k)$ decreases. The polaron band obtains a non–monotonic k–dependence as a consequence of the downward phonon dispersion. At $t_{\mathrm{ph}} = 0.4$ there is a notable deviation of the dispersive spectral weight at lowest ω from $E^{(0)}(k)$ around $k = 0.4\pi$ which is a consequence of the existence of MPEs just above $E^{(0)}(k)$.

In the intermediate coupling regime at $\lambda = 1.0$, see Figs. 5(f-j), we find an expected overall decrease of the polaron bandwidth in comparison to $\lambda = 0.5$ case, which is more pronounced at $t_{\mathrm{ph}} > 0$. The most prominent effect is the appearance of the dispersive spectral weight between the polaron band and the single phonon excitation $E_{1\mathrm{ph}}(k)$ which is due to two phonon excitations first observed at $t_{\mathrm{ph}} = 0.2$, presented in Fig. 5(h). At larger $t_{\mathrm{ph}} = 0.3$ it shifts down in energy and increases in the overall spectral weight, while at $t_{\mathrm{ph}} = 0.4$ we observe a broader dispersive spectral weight due to multiple (2, 4 possibly even 6) phonon excitations just above the polaron band. In the latter case a well defined quasiparticle peak is observed only in a narrow interval around the center of the Brillouin zone, consistent with the rapid decrease of Z_k seen in Fig. 2(d).

At smaller $\omega_0 = 0.5$ and $\lambda = 1$, presented in Fig. 6, we ob-

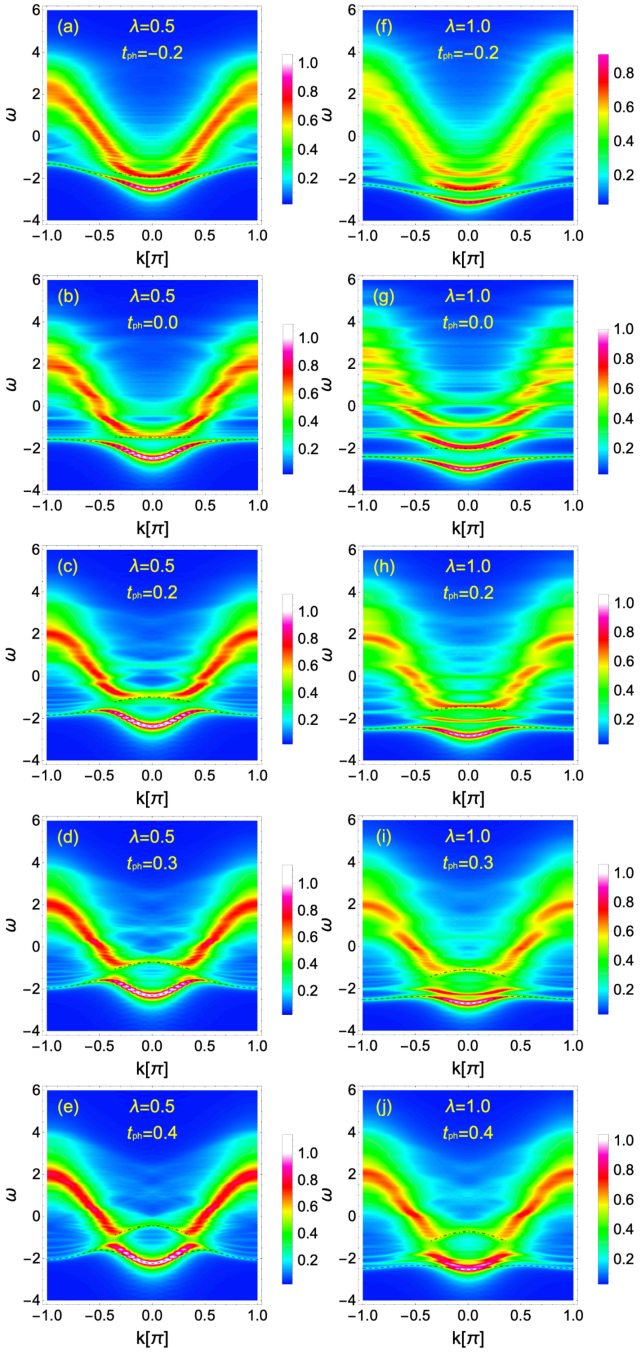

Figure 5: $A(\omega, k)$ computed at $\omega_0 = 1$ for different $t_{\rm ph}$ as denoted in legends where ω is in units of $t_{\rm el} = 1$. Dashed lines represent the lowest energy band $E^{(0)}(k)$ and dot-dashed lines at the center of the Brillouin zone represent the single phonon excitation, $E_{1\rm ph}(k)$. We have used artificial broadening $\eta = 0.05$. Identical colour coding has been used in all panels.

serve further flattening of the polaron band in comparison to $\omega_0 = 1$ case while the high-ω spectral weight is concentrated around the free electron band. In the dispersionless case, i.e. $t_{\rm ph} = 0.0$, two well defined bands, spaced by ω_0, are observed above the lowest energy polaron band. They represent polaron

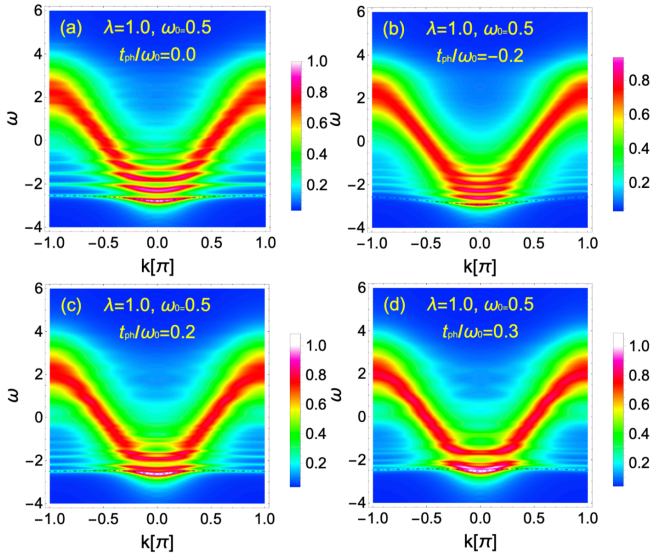

Figure 6: $A(\omega, k)$ computed at $\omega_0 = 0.5$ for different values of $t_{\rm ph}$ as denoted in legends where ω is in units of $t_{\rm el} = 1$. Dot–dashed lines represent the lowest energy band $E^{(0)}(k)$. We have used artificial broadening $\eta = 0.05$. Identical color coding has been used in all panels.

states with the addition of one- and two- phonon excitations. In the case of upward phonon dispersion, $t_{\rm ph} = -0.2$, the distance between low-ω bands decreases while additional bands appear around the middle of the Brillouin zone. Squeezing of bands is a result of the upward phonon dispersion since additional multi phonon excitations appear at lower energies in comparison to the dispersionless case. The opposite is expected to hold true in the case when $t_{\rm ph} > 0$, nevertheless, we observe additional structure just above the lowest energy polaron band that is in this case a consequence of multi–phonon processes from the edge of the Brillouin zone.

IV. CONCLUSIONS

Despite a body of work investigating various phenomena related to the electron phonon coupling based on the HM, the introduction of dispersion among optical phonons opens new pathways for future research in this field. Already a small amount of downward dispersion narrows the absorption spectrum in the frequency range of single phonon excitations. It also changes the dispersion of the polaron band as observed in the spectral function and narrows the frequency range where a strong quasiparticle peak is observed.

With increasing downward dispersion a MPE state appears as the lowest excited state of the system at zero momentum and even becomes the lowest energy state at finite momentum. The lower edge of the absorption spectrum shifts below the single phonon excitation frequency at zero momentum due to an electron scattering off an even number of MPEs from the edge of the Brillouin zone. Moreover, MPEs strongly influence the shape of the electron spectral function in the interme-

diate coupling regime. They emerge as a dispersive incoherent spectral weight below the single phonon excitation threshold just above the polaron band. Low–energy MPEs should be observable in systems with strong optical phonon dispersion in optical as well as angle resolved photoemission experiments.

It is important to stress that MPEs become the lowest excited states in the weak coupling limit at large optical phonon dispersion that may not be common in experimental systems. The analytical estimate for the threshold $t_{\rm ph}^{\rm th}(M_{\rm ph}=2)=\omega_0/6$ in the $\lambda\to 0$ limit yields the ratio $\omega(0)/\omega(\pi)=2$. With increasing λ the effective $t_{\rm ph}^{\rm th}(M_{\rm ph}=2)$ shifts towards smaller, physically more common values. In the case of $\lambda=1$ we obtain $t_{\rm ph}^{\rm th}(M_{\rm ph}=2)\sim 0.06$, which yields the ratio $\omega(0)/\omega(\pi)\sim 1.27$. Consequently, in the case of intermediate electron–phonon coupling, MPEs can be observed already at relatively small optical phonon dispersion. They remain observable even as the phonon dispersion is reduced. They may no longer be the lowest energy feature, but they are still there, with a singularity (van Hove) where they start to appear. The existence of low–energy MPEs may have a profound effect also on nonequilibrium[53–58] and finite–T properties[51] of electron–phonon coupled systems.

Acknowledgments

J.B. acknowledges the support by the program P1-0044 of the Slovenian Research Agency. J.B. and S.A.T. acknowledge support from the Center for Integrated Nanotechnologies, a U.S. Department of Energy, Office of Basic Energy Sciences user facility. S.A.T. acknowledges support from LDRD.

Appendix A: Efficiency of the numerical method

In Fig. A1 we demonstrate the efficiency of the method by plotting $A(\omega,k)$ for three different sizes of the Hilbert space. Apart from barely noticeable differences at higher ω results seem to have well converged.

In Fig. A2 we present comparison of $\sigma(\omega)$ at two distinct sets of parameters of the model and 4 different sizes of the Hilbert space. The dependence of results in terms of increasing sizes of the variational Hilbert space is more pronounced in the case of 'upward' phonon dispersion, i.e. for $t_{\rm ph}=-0.2$, where a multitude of peaks becomes denser as the system size increases. Even though the polaron is defined on an infinite 1-D lattice, the variational Hilbert space allows only a finite maximal distance between the electron and phonon excitation given by $L_{\rm max}=N_{\rm h}-1$, which consequently yields a discrete phonon spectrum $\omega(q)$.

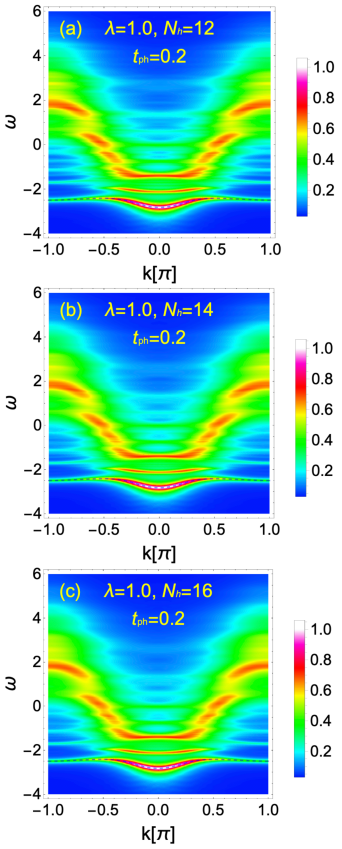

Figure A1: $A(\omega,k)$ computed at $\omega_0=1.0, \lambda=1.0, t_{\rm ph}=0.2$ computed using three different sizes of the Hilbert space ranging from $N_{\rm st}=10391$ for $N_{\rm h}=12$ in a), $N_{\rm st}=43310$ for $N_{\rm h}=14$ in b), through $N_{\rm st}=178617$ for $N_{\rm h}=16$ in c). The lowest energy band $E^{(0)}(k)$ is shown using dashed lines. We have used artificial broadening $\eta=0.05$. Identical color coding has been used in all panels.

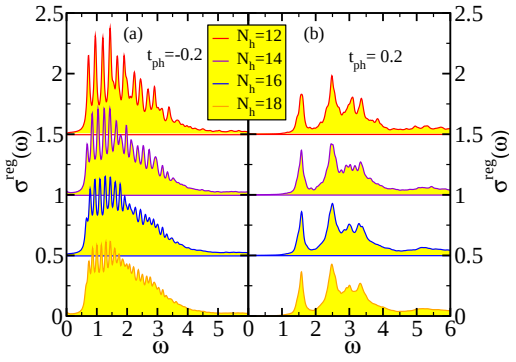

Figure A2: $\sigma(\omega)$ computed at $\omega_0=1.0, \lambda=1.0$ and $t_{\rm ph}=-0.2$ and 0.2 in a) and b), respectively. Systems sizes were from $N_{\rm st}=10391$ (many–body states per site) for $N_{\rm h}=12$ through $N_{\rm st}=731027$ for $N_{\rm h}=18$. We have used artificial broadening $\eta=0.05$.

Appendix B: $A(\omega)$ for a single site

In the case when $t_{\rm el} = 0$ the Hamiltonian in Eq. 1 is reduced to

$$H_{t_{\rm el}=0} = \sum_q \omega_q a_q^\dagger a_q + g\hat{n}_0(a_0^\dagger + a_0), \quad \text{(B1)}$$

which can be solved using a Lang–Firsov[59] transformation. In the case of a single electron on site 0, i.e. $n_0 = 1$, the ground state is given by[42]

$$|O\rangle = e^{-\sum_q \tilde{g}_q^2/2 - \tilde{g}_q a_q^\dagger} c_0^\dagger |\emptyset\rangle, \quad \text{(B2)}$$

where $\tilde{g}_q = \frac{g}{\sqrt{N_q \omega_q}}$, and excited states are obtained from

$$|\mathbf{m}\rangle = e^{-\sum_q \tilde{g}_q^2/2} \Pi_q \left(\frac{(a_q^\dagger + \tilde{g}_q)^{m_q}}{\sqrt{m_q!}} e^{-\tilde{g} a_q^\dagger} \right) c_0^\dagger |\emptyset\rangle \quad \text{(B3)}$$

where $|\mathbf{m}\rangle = |m_{q_1}, m_{q_2}, \ldots, m_{q_{N_q}}\rangle$. The energy spectrum is given by

$$\epsilon_{\mathbf{m}} = -\frac{1}{N_q} \sum_q \frac{g^2}{\omega_q} + \sum_q m_q \omega_q. \quad \text{(B4)}$$

Finally, $A(\omega)$ in Eq. 5 is obtained using the scalar product

$$|\langle \emptyset | c_0 | \mathbf{m} \rangle|^2 = e^{-\sum_q \tilde{g}_q^2} \Pi_q \frac{\tilde{g}_q^{2m_q}}{m_q!}. \quad \text{(B5)}$$

The analytical expression in Eq. 5 can be used to check the precision of our numerical approach using the variational Hilbert space. Comparison is given in Fig. B1.

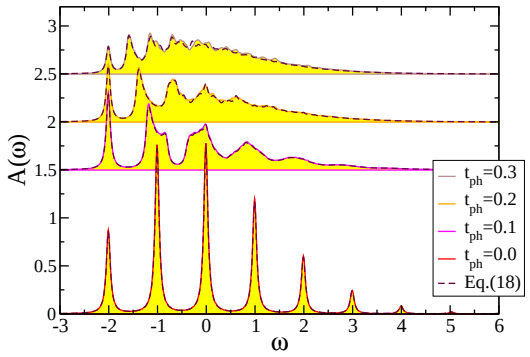

Figure B1: Comparison of $A(\omega)$ obtained using Lanczos approach with $t_{\rm el} = 0$ and $N_{\rm h} = 18$ presented with full lines and numerical summation of Eq. 5 shown in dashed lines. Parameters of the single–site model were $\omega_0 = 1$ and $g = \sqrt{2(\omega_0^2 - 4t_{\rm ph}^2)}$. In the latter case the product was performed using $N_q = 10$ equally spaced q values, $q = 2n\pi/N_q$, $n \in [1, \ldots, N_q]$, while the summation over different phonon quanta was limited to $m_{q_i} = [0, 1, 2, 3]$. In addition final results were averaged over shifted values q, i.e. $q \to q + \Delta q$ where $\Delta q = 2m\pi/(N_q * M_q)$, $m = 1, \ldots, M_q$ and $M_q = 4$. In both cases we have used artificial broadening $\eta = 0.05$.

[1] T. Holstein, Annals of Physics **8**, 325 (1959), ISSN 0003-4916, URL http://www.sciencedirect.com/science/article/pii/0003491659900028.

[2] G. Wellein and H. Fehske, Phys. Rev. B **56**, 4513 (1997).

[3] G. Wellein and H. Fehske, Phys. Rev. B **58**, 6208 (1998).

[4] J. Bonča, S. A. Trugman, and I. Batistić, Phys. Rev. B **60**, 1633 (1999).

[5] L. C. Ku, S. A. Trugman, and J. Bonča, Phys. Rev. B **65**, 174306 (2002).

[6] O. S. Barišić, Phys. Rev. B **65**, 144301 (2002), URL https://link.aps.org/doi/10.1103/PhysRevB.65.144301.

[7] O. S. Barišić, Phys. Rev. B **69**, 064302 (2004), URL https://link.aps.org/doi/10.1103/PhysRevB.69.064302.

[8] O. S. Barišić, Phys. Rev. B **73**, 214304 (2006), URL https://link.aps.org/doi/10.1103/PhysRevB.73.214304.

[9] G. De Filippis, V. Cataudella, V. M. Ramaglia, and C. A. Perroni, Phys. Rev. B **72**, 014307 (2005), URL https://link.aps.org/doi/10.1103/PhysRevB.72.014307.

[10] H. Fehske and S. A. Trugman, *Numerical Solution of the Holstein Polaron Problem* (Springer Netherlands, Dordrecht, 2007), pp. 393–461, ISBN 978-1-4020-6348-0, URL https://doi.org/10.1007/978-1-4020-6348-0_10.

[11] A. Alvermann, H. Fehske, and S. A. Trugman, Phys. Rev. B **81**, 165113 (2010), URL https://link.aps.org/doi/10.1103/PhysRevB.81.165113.

[12] T. Ohgoe and M. Imada, Phys. Rev. B **89**, 195139 (2014), URL https://link.aps.org/doi/10.1103/PhysRevB.89.195139.

[13] F. Dorfner, L. Vidmar, C. Brockt, E. Jeckelmann, and F. Heidrich-Meisner, Phys. Rev. B **91**, 104302 (2015), URL https://link.aps.org/doi/10.1103/PhysRevB.91.104302.

[14] J. H. Fetherolf, D. Golež, and T. C. Berkelbach, Phys. Rev. X **10**, 021062 (2020), URL https://link.aps.org/doi/10.1103/PhysRevX.10.021062.

[15] S. Engelsberg and J. R. Schrieffer, Phys. Rev. **131**, 993 (1963), URL https://link.aps.org/doi/10.1103/PhysRev.131.993.

[16] J. Loos, M. Hohenadler, A. Alvermann, and H. Fehske, Journal of Physics: Condensed Matter **18**, 7299 (2006), URL https://doi.org/10.1088%2F0953-8984%2F18%2F31%2F023.

[17] N. Prodanović and N. Vukmirović, Phys. Rev. B **99**, 104304 (2019), URL https://link.aps.org/doi/10.1103/PhysRevB.99.104304.

[18] M. Berciu, Phys. Rev. Lett. **97**, 036402 (2006), URL https://link.aps.org/doi/10.1103/PhysRevLett.97.036402.

[19] B. Lau, M. Berciu, and G. A. Sawatzky, Phys. Rev. B **76**, 174305 (2007).

[20] M. Berciu and G. L. Goodvin, Phys. Rev. B **76**, 165109 (2007).

[21] G. L. Goodvin, M. Berciu, and G. A. Sawatzky, Phys. Rev. B **74**, 245104 (2006).

[22] G. L. Goodvin, A. S. Mishchenko, and M. Berciu, Phys. Rev. Lett. **107**, 076403 (2011), URL https://link.aps.org/doi/10.1103/PhysRevLett.107.076403.

[23] J. Ranninger and U. Thibblin, Phys. Rev. B **45**, 7730 (1992), URL https://link.aps.org/doi/10.1103/PhysRevB.45.7730.

[24] F. Marsiglio, Physics Letters A **180**, 280 (1993).

[25] A. S. Alexandrov, V. V. Kabanov, and D. K. Ray, Phys. Rev. B **49**, 9915 (1994).

[26] H. Fehske, J. Loos, and G. Wellein, Zeitschrift für Physik B Condensed Matter **104**, 619 (1997), ISSN 1431-584X, URL https://doi.org/10.1007/s002570050498.

[27] B. Bäuml, G. Wellein, and H. Fehske, Phys. Rev. B **58**, 3663 (1998), URL https://link.aps.org/doi/10.1103/PhysRevB.58.3663.

[28] H. Fehske, J. Loos, and G. Wellein, Phys. Rev. B **61**, 8016 (2000), URL https://link.aps.org/doi/10.1103/PhysRevB.61.8016.

[29] M. Hohenadler, M. Aichhorn, and W. von der Linden, Phys. Rev. B **68**, 184304 (2003), URL https://link.aps.org/doi/10.1103/PhysRevB.68.184304.

[30] N. V. Prokof'ev and B. V. Svistunov, Phys. Rev. Lett. **81**, 2514 (1998), URL https://link.aps.org/doi/10.1103/PhysRevLett.81.2514.

[31] A. S. Alexandrov and P. E. Kornilovitch, Phys. Rev. Lett. **82**, 807 (1999), URL https://link.aps.org/doi/10.1103/PhysRevLett.82.807.

[32] V. Cataudella, G. D. Filippis, A. S. Mishchenko, and N. Nagaosa, Phys. Rev. Lett. **99**, 226402 (pages 4) (2007).

[33] F. F. Assaad, Phys. Rev. B **78**, 155124 (2008), URL https://link.aps.org/doi/10.1103/PhysRevB.78.155124.

[34] A. S. Mishchenko, N. Nagaosa, G. De Filippis, A. de Candia, and V. Cataudella, Phys. Rev. Lett. **114**, 146401 (2015), URL https://link.aps.org/doi/10.1103/PhysRevLett.114.146401.

[35] E. Jeckelmann and S. R. White, Phys. Rev. B **57**, 6376 (1998).

[36] C. Zhang, E. Jeckelmann, and S. R. White, Phys. Rev. B **60**, 14092 (1999), URL https://link.aps.org/doi/10.1103/PhysRevB.60.14092.

[37] D. Jansen, J. Bonča, and F. Heidrich-Meisner, Phys. Rev. B **102**, 165155 (2020), URL https://link.aps.org/doi/10.1103/PhysRevB.102.165155.

[38] S. Ciuchi, F. de Pasquale, S. Fratini, and D. Feinberg, Phys. Rev. B **56**, 4494 (1997), URL https://link.aps.org/doi/10.1103/PhysRevB.56.4494.

[39] S. Fratini and S. Ciuchi, Phys. Rev. B **74**, 075101 (2006), URL https://link.aps.org/doi/10.1103/PhysRevB.74.075101.

[40] Z. Li, C. J. Chandler, and F. Marsiglio, Phys. Rev. B **83**, 045104 (2011), URL https://link.aps.org/doi/10.1103/PhysRevB.83.045104.

[41] C. J. Chandler and F. Marsiglio, Phys. Rev. B **90**, 245149 (2014), URL https://link.aps.org/doi/10.1103/PhysRevB.90.245149.

[42] D. J. J. Marchand and M. Berciu, Phys. Rev. B **88**, 060301(R) (2013), URL https://link.aps.org/doi/10.1103/PhysRevB.88.060301.

[43] J. Bonča, S. A. Trugman, and M. Mierzejewski, Phys. Rev. B **97**, 174202 (2018), URL https://link.aps.org/doi/10.1103/PhysRevB.97.174202.

[44] N. C. Costa, T. Blommel, W.-T. Chiu, G. Batrouni, and R. T. Scalettar, Phys. Rev. Lett. **120**, 187003 (2018), URL https://link.aps.org/doi/10.1103/PhysRevLett.120.187003.

[45] M. Kang, S. W. Jung, W. J. Shin, Y. Sohn, S. H. Ryu, T. K. Kim, M. Hoesch, and K. S. Kim, Nature Materials **17**, 676 (2018), URL https://doi.org/10.1038/s41563-018-0092-7.

[46] B. Jusserand, D. Paquet, and F. Mollot, Phys. Rev. Lett. **63**, 2397 (1989), URL https://link.aps.org/doi/10.1103/PhysRevLett.63.2397.

[47] V. Y. Davydov, Y. E. Kitaev, I. N. Goncharuk, A. N. Smirnov, J. Graul, O. Semchinova, D. Uffmann, M. B. Smirnov, A. P. Mirgorodsky, and R. A. Evarestov, Phys. Rev. B **58**, 12899 (1998), URL https://link.aps.org/doi/10.1103/PhysRevB.58.12899.

[48] C. Lanczos, J. Res. Nat. Bur. Stand. **45**, 255 (1950).

[49] *The lowest energy of the one phonon state with total momentum k actually has the electron not with momentum zero, but with a small nonzero momentum q, and the phonon with momentum $k-q$, and similarly for two phonon states; for simplicity we neglect this small correction in this discussion.*

[50] *The system size is infinite, but the maximum distance allowed between the electron and the phonons is limited by the size of the hilbert space.*

[51] J. Bonča, S. A. Trugman, and M. Berciu, Phys. Rev. B **100**, 094307 (2019), URL https://link.aps.org/doi/10.1103/PhysRevB.100.094307.

[52] G. D. Mahan, *Many-Particle Physics* (Plenum Press, New York, 1990).

[53] D. Golež, J. Bonča, L. Vidmar, and S. A. Trugman, Phys. Rev. Lett. **109**, 236402 (2012), URL https://link.aps.org/doi/10.1103/PhysRevLett.109.236402.

[54] J. Kogoj, M. Mierzejewski, and J. Bonča, Phys. Rev. Lett. **117**, 227002 (2016), URL https://link.aps.org/doi/10.1103/PhysRevLett.117.227002.

[55] J. Kogoj, L. Vidmar, M. Mierzejewski, S. A. Trugman, and J. Bonča, Phys. Rev. B **94**, 014304 (2016), URL https://link.aps.org/doi/10.1103/PhysRevB.94.014304.

[56] Y. Murakami, P. Werner, N. Tsuji, and H. Aoki, Phys. Rev. B **91**, 045128 (2015), URL https://link.aps.org/doi/10.1103/PhysRevB.91.045128.

[57] Y. Murakami, P. Werner, N. Tsuji, and H. Aoki, Phys. Rev. B **93**, 094509 (2016), URL https://link.aps.org/doi/10.1103/PhysRevB.93.094509.

[58] Y. Murakami, P. Werner, N. Tsuji, and H. Aoki, Phys. Rev. B **94**, 115126 (2016), URL https://link.aps.org/doi/10.1103/PhysRevB.94.115126.

[59] I. G. Lang and Y. A. Firsov, Zh. Eksp. Teor. Fiz. **43**, 1843 (1962).